

# Superconductivity in iron sulfides intercalated by metal hydroxides

Xiuquan Zhou<sup>1,3</sup>, Christopher Eckberg<sup>2,3</sup>, Brandon Wilfong<sup>1,2</sup>, Sz-Chian Liou<sup>4</sup>, Hector K. Vivanco<sup>1</sup>, Johnpierre Paglione<sup>2,3</sup> and Efrain E. Rodriguez <sup>\*1,3</sup>

<sup>1</sup>Department of Chemistry and Biochemistry, University of Maryland, College Park, MD 20742

<sup>2</sup>Department of Physics, University of Maryland, College Park, MD 20742

<sup>3</sup>Center for Nanophysics and Advanced Materials, University of Maryland, College Park, MD 20742

<sup>4</sup>AIM Lab, Maryland NanoCenter, University of Maryland, College Park, MD 20742

Inspired by naturally occurring sulfide minerals, we present a new family of iron-based superconductors. A metastable form of FeS known as the mineral mackinawite forms two-dimensional sheets that can be readily intercalated by various cationic guest species. Under hydrothermal conditions using alkali metal hydroxides, we prepare two new superconducting phases including  $(\text{Li}_{1-x}\text{Fe}_x\text{OH})\text{FeS}$  and  $[(\text{Na}_{1-x}\text{Fe}_x)(\text{OH})_2]\text{FeS}$ . Superconducting layered heterostructures of  $[(\text{Na}_{1-x}\text{Fe}_x)(\text{OH})_2]\text{FeS}$  resemble incommensurate phases of the mineral tochilinite, which contains an iron square lattice interleaved with a hexagonal hydroxide lattice. Upon successful intercalation of the FeS layer, the critical temperature  $T_c$  of mackinawite is enhanced from 5 K to 8 K and 16 K for the  $(\text{Li}_{1-x}\text{Fe}_x\text{OH})^{\delta+}$  and  $[(\text{Na}_{1-x}\text{Fe}_x)(\text{OH})_2]^{\delta+}$  intercalates, respectively.

The chemistry of iron-based superconductors has been dominated by the arsenide and selenide compounds since their discovery nearly a decade ago.[1, 2] We demonstrate that iron sulfides prepared by hydrothermal routes provide a new series of superconductors that could further elucidate the structure-property relationships across closely related phases. Mainly, we isolate FeS layers to enhance their two-dimensional (2D) electronic character by inserting metal hydroxide spacers that also act as electron donating layers. The tetragonal form of FeS known as mackinawite is a metastable mineral recently shown to be superconducting with a  $T_c$  near 4 K.[3, 4] Mackinawite FeS adopts the anti-PbO structure where  $\text{FeS}_4$  tetrahedra edge-share to form 2D layers held by weak van der Waals interactions. Consequently, these layered chalcogenides are excellent hosts for intercalation chemistry.[5] In the selenide case, the  $T_c$  can be increased from 8 K[2] to 42-44 K by intercalation of alkali metal in liquid ammonia[6, 7] or

---

\*efrain@umd.edu

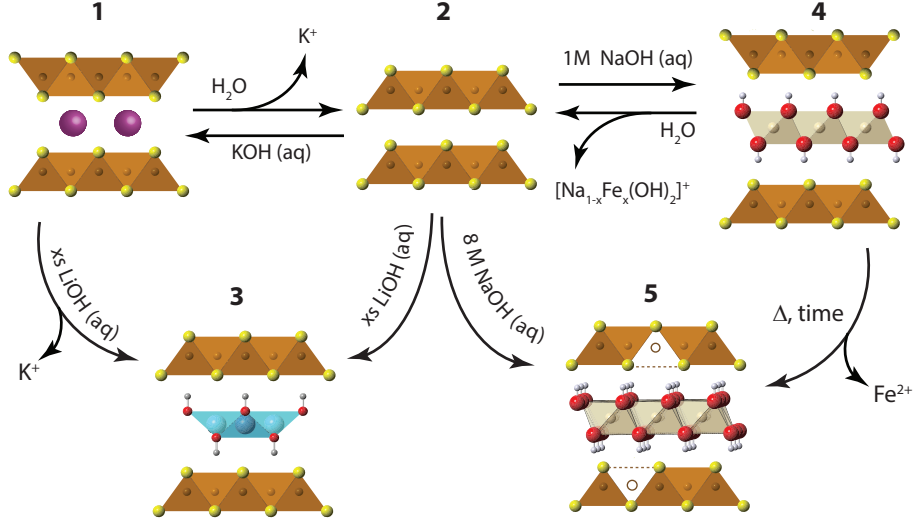


Figure 1: Synthetic scheme for the intercalation chemistry of FeS with metal hydroxides and  $K^+$  cations via hydrothermal preparations.

$(Li_{1-x}Fe_xOH)^{\delta+}$  under hydrothermal conditions.[8, 9] Therefore, our goal was to extend this type of chemistry to the sulfides.

We have found the intercalation chemistry of layered FeS to be quite versatile, and we illustrate in Fig. 1 the various guest-host phases that can be prepared via hydrothermal routes. Inspired by recent studies on the hydrothermally prepared 42 K superconductor,  $(Li_{1-x}Fe_xOH)FeSe$ , [8–11] we applied similar intercalation chemistry for FeS using different alkali metal hydroxides. Herein, we report newfound superconductivity in the LiOH- and NaOH-intercalated FeS systems. We find that the superconducting properties depend on preserving an iron square lattice and in electron doping the metallic FeS layer. Detailed conditions for each step of Fig. 1 can be found in Supplementary Information.

We first describe our results utilizing LiOH to intercalate the FeS host. Our starting point is to utilize  $K_xFe_{2-y}S_2$  (**1**) crystals grown from congruently melting the constituent elements. Under hydrothermal and basic conditions, these crystals can either de-intercalate the potassium cations to form mackinawite FeS (**2**), or cation exchange the potassium for cationic layers of  $(Li_{1-x}Fe_xOH)^{\delta+}$  as traced in the reaction from **1** to **3**. Alternatively, we can isolate  $(Li_{1-x}Fe_xOH)FeS$  (**3**) via the method used by previous workers, [9, 12, 13] whereby polycrystalline material is prepared by the oxidation of iron metal in the presence of a sulfide source and excess amounts of LiOH base. In this reaction (**2** to **3** in Fig. 1), mackinawite FeS forms in-situ with the hydroxide layers to yield  $(Li_{1-x}Fe_xOH)FeS$ . We note that Lu *et al.* [12] and Pachmayr *et al.* [9] had previously observed superconductivity in some of their mixed solid-solutions,  $(Li_{1-x}Fe_xOH)FeS_{1-z}Se_z$ , but both studies had concluded that their pure sulfide samples ( $z = 0$ ) were nonsuperconducting.

We found that superconductivity can be established in the intercalated sulfides for both our cation exchange and polycrystalline routes if two conditions are met: 1) the reaction temperature must be less than 160 °C, i.e. mild hy-

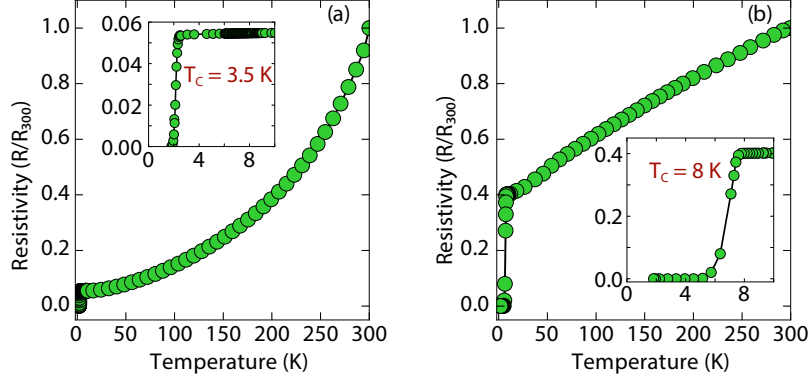


Figure 2: Temperature dependent electrical resistivity of superconducting  $(\text{Li}_{1-x}\text{Fe}_x\text{OH})\text{FeS}$  samples prepared via the cation exchange route with (a) thiourea and (b)  $\text{Na}_2\text{S} \cdot 9\text{H}_2\text{O}$ , respectively.

drothermal conditions, and 2) the environment must remain reducing. The latter condition was maintained by the inclusion of tin metal plate as a way to dynamically change the conditions from oxidizing to more reducing.[11] No tin was found in the products as determined from energy dispersive X-ray spectroscopy (EDS).

Magnetization and electrical resistivity measurements revealed that the  $T_c$  of the  $(\text{Li}_{1-x}\text{Fe}_x\text{OH})\text{FeS}$  phases can vary from 3 K to 8 K, with some samples showing superconducting volume fractions up to 40%, indicative of bulk superconductivity (Fig. S1). We must note, however, that due to the proximity of  $T_c$  to the base temperature of our magnetometer (1.8 K) we could not reach full saturation of the diamagnetic signal. Therefore, it is possible that the volume fraction is even higher than 40%.

Remarkably, for  $(\text{Li}_{1-x}\text{Fe}_x\text{OH})\text{FeS}$  samples prepared via the cation exchange route, we observed  $T_c$ 's both above and below that of bulk FeS (Fig. 2). This result indicates that charge doping into the FeS layer is controlling the critical temperatures in  $(\text{Li}_{1-x}\text{Fe}_x\text{OH})\text{FeS}$ . From our various samples, intercalation by  $(\text{Li}_{1-x}\text{Fe}_x\text{OH})^{\delta+}$  could increase the  $T_c$  of FeS up to 8 K. The upper critical field ( $H_{c2}$ ) of the sample for  $H \parallel c$  at 1.8 K is 220 Oe (Fig. S2), which is smaller to that of FeS (0.16 T).[4]

It is also interesting to note that the superconducting sample with the lower  $T_c$  ( $\approx 3.5$  K) showed a  $T^2$ -dependence in its normal state electrical resistivity (Fig. 2a). Typically,  $T^2$  dependence is associated with Fermi liquid behavior, and the sample with the lower  $T_c$  exhibits this type of electronic behavior more pronouncedly (Fig. 2). Fermi liquid behavior has been observed in cuprate superconductors with hole overdoping,[14]. Therefore, it is possible that both the lower  $T_c$  and  $T^2$ -behavior for the sample presented in Fig. 2a are related to having non-optimal charge doping in the FeS layers.

To determine the structure of our superconducting  $(\text{Li}_{1-x}\text{Fe}_x\text{OH})\text{FeS}$  samples, we performed high-resolution synchrotron X-ray powder diffraction (sXRD) as shown in Fig. 3. From quantitative analysis of the data, we have provided detailed crystallographic information for two samples in Supplementary Infor-

mation (Table S1). Upon intercalation, the Fe-Fe bond distances increased from 2.604 Å in bulk FeS[11] to 2.619 Å, but the FeS<sub>4</sub> tetrahedron remains virtually unchanged both in bond distances and bond angles. There is also an increase in the distance between the iron square sublattices. In mackinawite, that interlayer distance is  $\approx 5.03$  Å,[4] whereas in the (Li<sub>1-x</sub>Fe<sub>x</sub>OH)-intercalated phase it is 8.89 Å–8.93 Å, further enhancing the two-dimensionality of its electronic structure. Due to the subtle changes in the (Li<sub>1-x</sub>Fe<sub>x</sub>OH)<sup>δ+</sup> layer, Rietveld refinements for the superconducting and non-superconducting samples did not show significant differences in their stoichiometries (both close to (Li<sub>0.85</sub>Fe<sub>0.15</sub>OH)FeS).

For a more accurate analysis of chemical composition of the (Li<sub>1-x</sub>Fe<sub>x</sub>OH)FeS phases, we performed inductively coupled plasma atomic emission spectroscopy (ICP-AES). For superconducting and non-superconducting samples, ICP-AES afforded Fe/Li ratios of 1.132 and 1.093, respectively. Therefore, the superconducting samples contains more Fe in the hydroxide layer and consequently more electron doping in the FeS layer. In our earlier work on the phase diagram of the selenide analogues, we found that higher  $T_c$ 's were achieved with lower reaction temperatures so that more iron cations could incorporate into the metal hydroxide layer.[11] Studies on the same system by Clarke *et al.* demonstrated that the iron in the hydroxide layer is Fe<sup>2+</sup> and that iron vacancies in the FeSe layer degraded the superconducting properties.[10] Through the cation exchange method demonstrated here, vacancy formation in the FeS layer is less of a factor and achieving sufficient electron doping from the hydroxide layer is the bigger challenge. We detail in Table S2 (Supplementary Information) the synthesis conditions for various superconducting and non-superconducting samples.

Our next objective was to explore larger alkali metal hydroxides as intercalates. Unlike LiOH, which favors a square lattice commensurate with that of mackinawite FeS, a similar structure for NaOH was not reproduced. Instead, we found a new phase with very few reflections in the XRD powder pattern and its first peak corresponded to a  $d$ -spacing of 5.38 Å. This phase is reminiscent of a natural mineral known as tochilinite, which consists of brucite-type Mg(OH)<sub>2</sub> layers between mackinawite-like FeS sheets. Natural tochilinite is quasi-commensurate and its (001) reflection has a  $d$ -spacing of 10.72 Å, which is close to twice our first reflection. Therefore, if the first peak of our new phase is the (002) reflection, it would indicate that the FeS layers are stacked in a body-centered fashion. Since we only observe (00 $l$ ) reflections in our new phase, the square and hexagonal sheets are completely incommensurate to each other in the  $ab$ -plane. Henceforth, we refer to this phase as *inc*-Na-tochilinite (4 in Fig 1).

We found the new *inc*-Na-tochilinite to always coexist with some residual mackinawite FeS (Fig. S3), but only samples with *inc*-Na-tochilinite displayed superconductivity below  $\approx 16$  K as seen from magnetization measurements (Fig. 4). The ratio between *inc*-Na-tochilinite and mackinawite FeS was increased by using less Na<sub>2</sub>S · 9H<sub>2</sub>O and decreased with prolonged ultrasonication, indicating conversion to FeS by de-intercalation. The equilibrium between the two phases is indicated in the steps between 2 and 4 in Fig. 1. For a sample that contained less *inc*-Na-tochilinite (Fig. S3), we observed two transitions at 5 K and 16 K (Fig. S4), corresponding to mackinawite FeS and *inc*-Na-tochilinite, respectively.

Magnetization versus field measurements of samples containing *inc*-Na-tochilinite revealed an  $H_{c2}$  of about 330 Oe (Fig. 4b). Interestingly, we also observed some

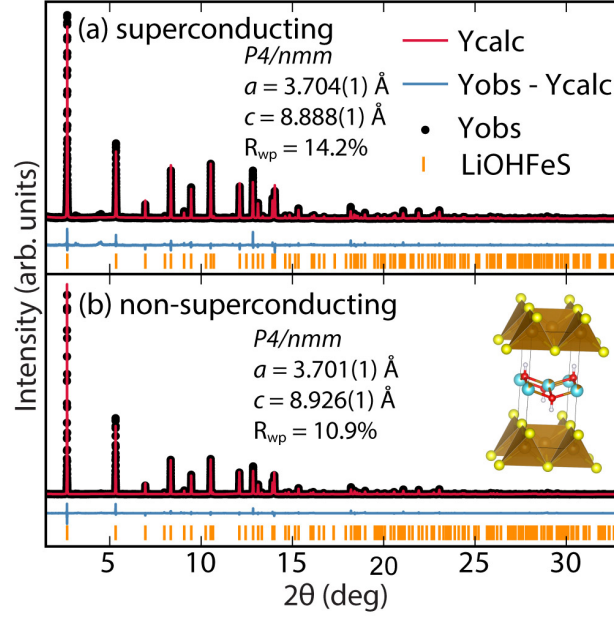


Figure 3: Synchrotron XRD patterns of (a) superconducting and (b) non-superconducting  $(\text{Li}_{1-x}\text{Fe}_x\text{OH})\text{FeS}$  prepared via in-situ formation at 160 °C and 200 °C, respectively.

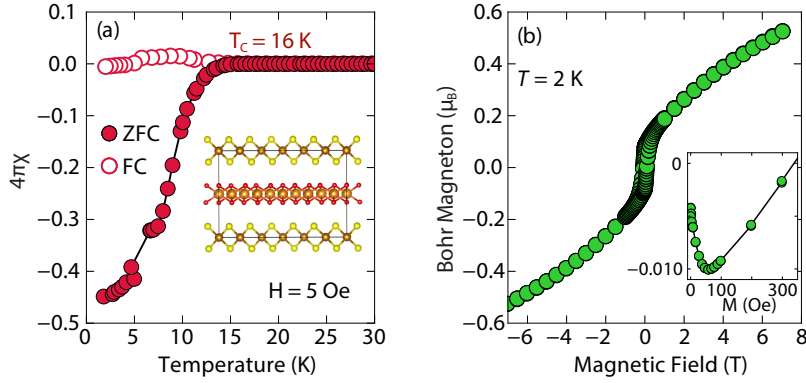


Figure 4: Magnetic susceptibility measurements of *inc*-Na-tochilinite as a function of (a) temperature and (b) field. The insert in (b) shows a zoomed region between 0 and 350 Oe, and it indicates diamagnetic behavior under low field and an  $H_{c2}$  of 330 Oe.

hysteresis for its normal state properties at high field. The coexistence of superconductivity and ferromagnetism was previously observed in the  $(\text{Li}_{1-x}\text{Fe}_x\text{OH})\text{FeSe}$  system, and the ferromagnetism was suggested to arise from the iron cations partially substituted on the Li site.[11, 15, 16] Considering the synthetic and structural proximity between the reported  $(\text{Li}_{1-x}\text{Fe}_x\text{OH})\text{FeSe}$ [11] and the present

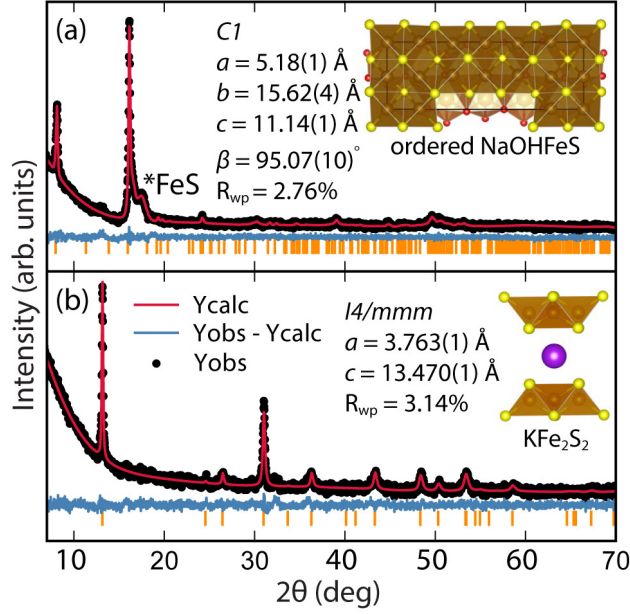


Figure 5: XRD patterns of hydrothermally prepared (a) Na-tochilinite and (b)  $K_x\text{Fe}_{2-y}\text{S}_2$ , respectively.

$[(\text{Na}_{1-x}\text{Fe}_x)(\text{OH})_2]\text{FeS}$  system, it is possible that the magnetism in this new compound originates from Fe cations in the hydroxide layer.

The argument for *inc*-Na-tochilinite as the superconducting phase is further strengthened by the stabilization of a non-superconducting tochilinite that is quasi-commensurate (Fig. 5a), which we refer to as Na-tochilinite. This non-superconducting phase was prepared by utilizing more concentrated solutions of NaOH (5 to 8 M) in the hydrothermal reactions. Significantly less tetragonal FeS was recovered (Fig. 5a) with Na-tochilinite, and this phase did not easily revert to FeS by ultrasonication, indicating its stability with respect to *inc*-Na-tochilinite. Using the crystal structure of the naturally occurring mineral known as ferrotouchilinite  $(2(\text{Fe}_{1-x}\text{S}) \cdot 1.8[(\text{Mg}, \text{Fe})(\text{OH})_2])$ , [17] with lattice parameters,  $a = 5.37 \text{ \AA}$ ,  $b = 15.65 \text{ \AA}$ ,  $c = 10.72 \text{ \AA}$ , we extracted by Pawley fits the lattice parameters of our Na-tochilinite (Fig. 5a)

Given the difficulty in elucidating the structure of these heterolayered materials by powder XRD, we have also performed transmission electron diffraction (ED). We present two ED patterns with the  $(hk0)$  reflections that were difficult to resolve from powder XRD—one for mackinawite FeS and the other for Na-tochilinite. Along the  $[001]$  zone axis, the ED pattern of FeS (Fig. 6a) clearly demonstrates a square lattice corresponding to its simple primitive tetragonal structure. For Na-tochilinite, additional satellite reflections emerge in addition to the square lattice of FeS (Fig. 6b). Upon closer inspection the seemingly 4-fold symmetry of the brighter reflections in Na-tochilinite is actually a 2-fold axis. The angle between the cross-sections connecting the  $(200)$  to  $(\bar{2}00)$  and  $(060)$  to  $(0\bar{6}0)$  is about  $93^\circ$ , which is close to the monoclinic angle found from XRD ( $\beta = 95.07(10)^\circ$ ). Therefore, the monoclinic distortion of the FeS square



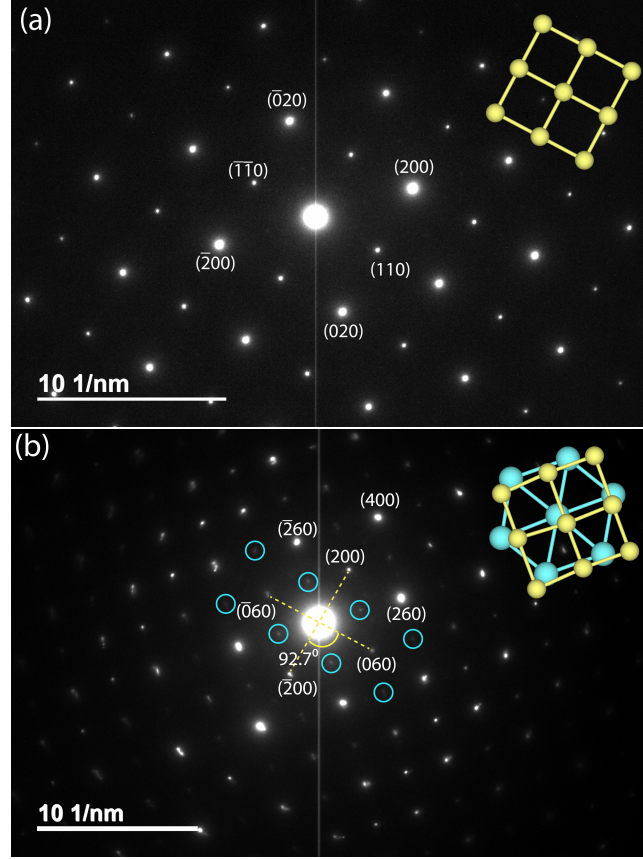


Figure 6: Electron diffraction patterns along the zone axis [001] of (a) FeS and (b) Na-tochilinite, respectively. Some weak diffraction spots of Na-Tochilinite are highlighted by blue circles. Projections of tetragonal and hexagonal lattices are shown in yellow and blue, respectively.

lattice in Na-tochilinite is clearly reproduced in the ED along with the satellite reflections indicating the intercalation of the FeS layers. The lattice constants  $a$  and  $b$  extracted from ED are 5.2(2) Å and 15.9(2) Å, respectively—in good agreement with the XRD analysis ( $a = 5.18(1)$  Å and  $b = 15.62(4)$  Å).

Next, we discuss the nature of the chemical composition of Na-tochilinite. As in some natural minerals, [18] we can formulate the stoichiometry as  $[(\text{Na}_{1-x}\text{Fe}_x)(\text{OH})_2]\text{FeS}$ , and ICP-AES analysis provided an Fe/Na ratio of 2.99. Therefore,  $[(\text{Na}_{0.5}\text{Fe}_{0.5})(\text{OH})_2]\text{FeS}$  is the proposed chemical formula since  $(1 + x)/(1 - x) = 2.99$ . This result suggests the presence of large amounts of  $\text{Fe}^{3+}$  in the hydroxide layers in Na-tochilinite to balance the charges with two  $\text{OH}^-$  groups. While ICP-AES could not determine the number of hydroxide groups, crystal chemical reasoning supports  $M(\text{OH})_2$  for the spacer layer since this is how the hexagonal brucite is formulated. Furthermore, the highly reactive and pyrophoric mineral known as “white rust” consists of  $\text{Fe}(\text{OH})_2$  layers that crystallize in the  $\text{CdI}_2$ -type structure.[19] By oxidizing to  $\text{Fe}^{3+}$ , such a layer would be stabilized by the presence of either  $\text{Na}^+$  or vacancies, and indeed natural tochilinites exhibit sig-

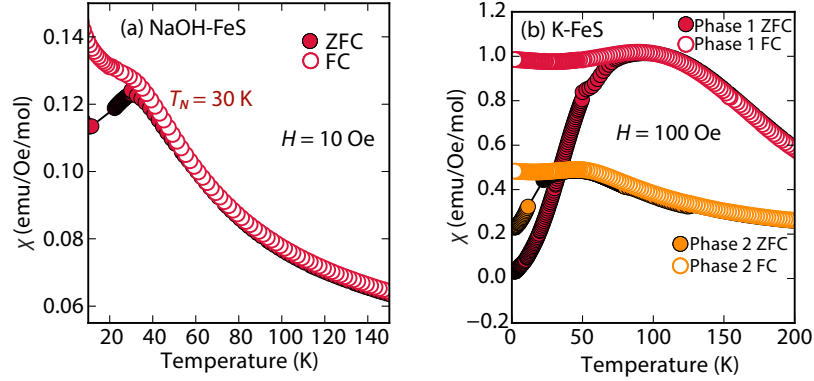


Figure 7: Magnetic susceptibility measurements of (a) Na-tochilinite and (b)  $K_xFe_{2-y}S_2$ , respectively. The lattice constant  $c$  for Phase 1 and Phase 2 in (b) is 13.627 and 13.470 Å, respectively.

nificant amounts of Fe vacancies (up to 20%).[20, 21]

The presence of iron vacancies and distortion of the iron square sublattice are the reasons that Na-tochilinite is not superconducting. Rather, it displays broad features in the magnetization reminiscent of short-range antiferromagnetic behavior. Interestingly, Parise *et al.* found through neutron diffraction that the  $Fe(OH)_2$  exhibits long-range magnetic ordering with each sheet consisting of ferromagnetically coupled iron centers, and each sheet anti-aligned to each other.[19] Future neutron diffraction experiments on both superconducting and non-superconducting tochilinites would reveal the nature of the interesting magnetic ordering arising from the hydroxide layer.

Efforts to incorporate KOH layers into FeS hosts resulted in cationic  $K^+$  intercalation instead. When hydrothermal reactions of Fe powder with KOH and a sulfide source were undertaken, the XRD pattern revealed a phase pure sample similar to the  $K_xFe_{2-y}S_2$  prepared using solid-state routes (Fig. 5b). In addition, its pattern could be well fit by Rietveld refinement using the crystal structure of  $K_xFe_{2-y}S_2$  with the space group  $I4/mmm$ . Its layer spacing (lattice constant  $c$ ) is 13.47 Å, which is comparable to the reported 245-type ( $I4/m$ , 13.599 Å)[22] and 122-type ( $I4/mmm$ , 13.546 Å) compounds.[23]. EDS analysis gave a composition of  $K_{1.1}Fe_{1.6}S_2$  and its magnetic susceptibility displayed broad antiferromagnetic transitions around 45 K ( $c = 13.470$  Å) and 96 K ( $c = 13.627$  Å) for samples with different layer spacings (Fig. 7b). Since the transitions are so broad, it is likely that long-range antiferromagnetic ordering is never observed but rather some form of low-dimensional antiferromagnetic behavior. Nevertheless, it is remarkable that we could prepare via hydrothermal routes such ternary phases since these have typically been prepared by conventional solid state techniques.

In conclusion, we have demonstrated that metal hydroxides can be intercalated into tetragonal mackinawite-type FeS via hydrothermal routes, and that new superconductors can be prepared in this manner. Given that FeS is a metastable phase, it is of paramount importance that we continue to explore novel low temperature routes towards mineral-inspired superconductors. While



we have enhanced  $T_c$  to 16 K through these charge-doping hydroxide layers, we have also demonstrated that FeS can serve as a suitable host for various guests species acting as bases. The differences in going from  $\text{Li}^+$  to  $\text{Na}^+$  to  $\text{K}^+$  are remarkable in the vastly different structure types that were stabilized. These results point to the exciting possibility of utilizing both size and charge parameters of other guests species, such as amines, to ultimately enhance the superconductivity of sulfide-based materials. Furthermore, the fact that heterostructures could be stabilized points to mackinawite-type FeS as a possible new 2D chalcogenide to be incorporated into other functional 2D materials. The field of vertical 2D heterostructures has exciting possibilities for constructing entirely new functional materials,<sup>[24]</sup> and mackinawite-type FeS could be a new building block in such structures.

## Experimental Section

All Samples in this work were prepared using the hydrothermal method described in detail from an earlier work.<sup>[11]</sup> Detailed synthetic conditions for samples presented in this work are described in Supplementary Information. Powder X-ray diffraction (XRD) data were collected using a Bruker D8 X-ray diffractometer with Cu  $K\alpha$  radiation,  $\lambda = 1.5418 \text{ \AA}$ . High-resolution synchrotron X-ray diffraction were carried out at Beamline 11-BM at the Advanced Photon Source (APS). Diffraction data were collected between  $0.5^\circ$  and  $46^\circ$  with a step size of  $0.0001^\circ$  using a constant wavelength  $\lambda = 0.414164 \text{ \AA}$  (30 keV). Rietveld and Pawley refinements were carried out using TOPAS software.<sup>[25]</sup> Microscopic images were examined on a Hitachi SU-70 SEM field emission scanning electron microscope (SEM), and their elemental compositions were determined by energy dispersive X-ray spectroscopy (EDS) using a BRUKER EDS detector. Electron diffraction patterns were obtained using a JEM 2100 LaB6 transmission electron microscope (TEM) at an acceleration voltage of 200 KeV. Inductively coupled plasma atomic emission spectroscopy (ICP-AES) data were collected using an Shimadzu ICPE-9000 spectrometer. Standards used for ICP-AES were diluted from 1000 ppm of respective elements purchased from FLUKA. Magnetic susceptibility measurements were performed using a Quantum Design Magnetic Properties Measurement System (MPMS). Electrical resistivity measurements were performed on a 14 T Quantum Design Physical Properties Measurement System (PPMS).

## Acknowledgements

Research at the University of Maryland was supported by the NSF Career DMR-1455118 and the AFOSR Grant No. FA9550-14-1-0332. Use of the Advanced Photon Source at Argonne National Laboratory was supported by the U. S. Department of Energy, Office of Science, Office of Basic Energy Sciences, under Contract No. DE-AC02-06CH11357. We also acknowledge support from the Center for Nanophysics and Advanced Materials.

## References

- [1] Y. Kamihara, H. Hiramatsu, M. Hirano, R. Kawamura, H. Yanagi, T. Kamiya, H. Hosono, *Journal of the American Chemical Society* **2006**, *128*, 10012–10013
- [2] F.-C. Hsu, J.-Y. Luo, K.-W. Yeh, T.-K. Chen, T.-W. Huang, P. M. Wu, Y.-C. Lee, Y.-L. Huang, Y.-Y. Chu, D.-C. Yan, M.-K. Wu, *Proceedings of the National Academy of Sciences* **2008**, *105*, 14262–14264
- [3] X. Lai, H. Zhang, Y. Wang, X. Wang, X. Zhang, J. Lin, F. Huang, *Journal of the American Chemical Society* **2015**, *137*, 10148–10151
- [4] C. K. H. Borg, X. Zhou, C. Eckberg, D. J. Campbell, S. R. Saha, J. Paglione, E. E. Rodriguez, *Phys. Rev. B* **2016**, *93*, 094522
- [5] H. K. Vivanco, E. E. Rodriguez, *Journal of Solid State Chemistry* **2016**, –
- [6] M. Burrard-Lucas, D. G. Free, S. J. Sedlmaier, J. D. Wright, S. J. Cassidy, Y. Hara, A. J. Corkett, T. Lancaster, P. J. Baker, S. J. Blundell, S. J. Clarke, *Nat. Mater.* **2013**, *12*, 15–19
- [7] T. Ying, X. Chen, G. Wang, S. Jin, X. Lai, T. Zhou, H. Zhang, S. Shen, W. Wang, *Journal of the American Chemical Society* **2013**, *135*, 2951–2954
- [8] X. F. Lu, N. Z. Wang, G. H. Zhang, X. G. Luo, Z. M. Ma, B. Lei, F. Q. Huang, X. H. Chen, *Phys. Rev. B* **2014**, *89*, 020507
- [9] U. Pachmayr, D. Johrendt, *Chem. Commun.* **2015**, *51*, 4689–4692
- [10] H. Sun, D. N. Woodruff, S. J. Cassidy, G. M. Allcroft, S. J. Sedlmaier, A. L. Thompson, P. A. Bingham, S. D. Forder, S. Cartenet, N. Mary, S. Ramos, F. R. Foronda, B. H. Williams, X. Li, S. J. Blundell, S. J. Clarke, *Inorganic Chemistry* **2015**, *54*, 1958–1964
- [11] X. Zhou, C. K. H. Borg, J. W. Lynn, S. R. Saha, J. Paglione, E. E. Rodriguez, *J. Mater. Chem. C* **2016**, *4*, 3934–3941
- [12] X. F. Lu, N. Z. Wang, X. G. Luo, G. H. Zhang, X. L. Gong, F. Q. Huang, X. H. Chen, *Phys. Rev. B* **2014**, *90*, 214520
- [13] X. Zhang, X. Lai, N. Yi, J. He, H. Chen, H. Zhang, J. Lin, F. Huang, *RSC Adv.* **2015**, *5*, 38248–38253
- [14] K. Levin, J. H. Kim, J. Lu, Q. Si, *Physica C: Superconductivity* **1991**, *175*, 449 – 522
- [15] U. Pachmayr, F. Nitsche, H. Luetkens, S. Kamusella, F. Brückner, R. Sarkar, H.-H. Klauss, D. Johrendt, *Angewandte Chemie International Edition* **2015**, *54*, 293–297
- [16] J. W. Lynn, X. Zhou, C. K. H. Borg, S. R. Saha, J. Paglione, E. E. Rodriguez, *Phys. Rev. B* **2015**, *92*, 060510
- [17] N. Organova, V. Drits, A. Dmitrik, *Soviet Physics Crystallography* **1972**, *17*, 667

- [18] I. V. Pekov, E. V. Sereda, Y. S. Polekhovsky, S. N. Britvin, N. V. Chukanov, V. O. Yapaskurt, I. A. Bryzgalov, *Geology of Ore Deposits* **2013**, *55*, 567–574
- [19] J. B. Parise, W. G. Marshall, R. I. Smith, H. D. Lutz, H. Möller, *American Mineralogist* **2000**, *85*, 189–193
- [20] Y. Peng, G. Xi, C. Zhong, L. Wang, J. Lu, X. Sun, L. Zhu, Q. Han, L. Chen, L. Shi, M. Sun, Q. Li, M. Yu, M. Yin, *Geochim. Cosmochim. Acta* **2009**, *73*, 4862 – 4878
- [21] G. A. Kakos, T. W. Turney, T. B. Williams, *Journal of Solid State Chemistry* **1994**, *108*, 102 – 111
- [22] H. Lei, M. Abeykoon, E. S. Bozin, C. Petrovic, *Phys. Rev. B* **2011**, *83*, 180503
- [23] J. J. Ying, Z. J. Xiang, Z. Y. Li, Y. J. Yan, M. Zhang, A. F. Wang, X. G. Luo, X. H. Chen, *Phys. Rev. B* **2012**, *85*, 054506
- [24] B. V. Lotsch, *Annual Review of Materials Research* **2015**, *45*, 85–109
- [25] R. W. Cheary, A. Coelho, *J. Appl. Crystallogr.* **1992**, *25*, 109–121

# Supplementary Information

## Synthetic conditions

For a typical preparation of  $(\text{Li}_{1-x}\text{Fe}_x\text{OH})\text{FeS}$  via the in-situ formation route (from **2** to **3** in Fig. 1), 5 mmol Fe powder, 8 mmol of  $\text{Li}_2\text{S}$  (or thiourea/ $\text{Na}_2\text{S} \cdot 9\text{H}_2\text{O}$ ), 1 mmol Sn metal plate and 72 mmol  $\text{LiOH} \cdot \text{H}_2\text{O}$  were mixed with 10 mL de-ionized (DI) water in a Teflon-lined stainless steel autoclave at 120-200 °C for 3 days. Mainly  $\text{Li}_2\text{S}$  was used as the sulfur source to avoid possible interference from sodium. Afterwards, the content in the autoclave was washed and centrifuged several times until the supernatant was clear. The remaining product was collected, vacuumed dried, and stored in a nitrogen-filled glove box.

For  $(\text{Li}_{1-x}\text{Fe}_x\text{OH})\text{FeS}$  prepared via the cation exchange route (from **1** to **3** in Fig. 1),  $\text{K}_x\text{Fe}_{2-y}\text{S}_2$  single crystals grown from high temperature, 3 mmol Fe powder, 3 mmol of sulfur source ( $\text{Li}_2\text{S}$ , thiourea or  $\text{Na}_2\text{S} \cdot 9\text{H}_2\text{O}$ ), 1 mmol Sn metal plate and 72 mmol  $\text{LiOH} \cdot \text{H}_2\text{O}$  were used as starting materials for similar hydrothermal reaction at 120 °C for 1-3 days. For the growth of the  $\text{K}_x\text{Fe}_{2-y}\text{S}_2$  single crystals, 1.2 g of FeS powder was mixed with 0.266 g of potassium metal to match the nominal composition of  $\text{KFe}_2\text{S}_2$ . The FeS/K mixtures were loaded in a quartz ampoule inside a nitrogen-filled glovebox, and the ampoules flame sealed under vacuum. In order to avoid oxidation of the samples from breaking of the ampoule due to potassium-induced corrosion of the quartz walls, the sample container was sealed in a larger ampoule. For crystal growth of  $\text{K}_x\text{Fe}_{2-y}\text{S}_2$ , the mixture was heated to 1030 °C over 10 h and held at 1030 °C for 3 hours to form a homogeneous melt. Subsequently, the melt was slowly cooled at a rate of 6 °C/hour to 650 °C to allow crystal growth.

Superconducting *inc*-Na-tochinilite was prepared with 10 mmol Fe powder, 10-12 mmol  $\text{Na}_2\text{S} \cdot 9\text{H}_2\text{O}$ , 5-10 mmol NaOH and 10 mL DI water in an autoclave at 120 °C for 7 days. The non-superconducting Na-Tochilinite was prepared with 10 mmol Fe powder, 15-20 mmol  $\text{Na}_2\text{S} \cdot 9\text{H}_2\text{O}$ , 50-80 mmol NaOH, 2 mmol Sn metal plate and 10 mL DI water in an autoclave at 120 °C for 3-7 days.  $\text{K}_x\text{Fe}_{2-y}\text{S}_2$  powders were prepared with 10 mmol Fe powder, 15 mmol thiourea, 50-100 mmol KOH, 2mmol Sn metal plate and 10 mL DI water in an autoclave at 160 °C for 5-7 days.

## More notes on the $\text{K}_x\text{Fe}_{2-y}\text{S}_2$ phase

While we did not find superconducting phases containing potassium, we did demonstrate that the synthetic temperature for the preparation of  $\text{K}_x\text{Fe}_{2-y}\text{S}_2$  can be lowered from about 1000 °C to 160 °C through hydrothermal methods. Without KOH, single crystals of  $\text{K}_x\text{Fe}_{2-y}\text{S}_2$  can be completely converted to mackinawite FeS. Therefore, the conversion between  $\text{K}_x\text{Fe}_{2-y}\text{S}_2$  and tetragonal FeS is fully reversible, as traced by the equilibrium reaction between **1** and **2** in Fig. 1. With further work on reducing the iron vacancies, the potassium intercalated phases could be made superconducting. To confirm this, we started

to apply this route to the selenide system without optimization, and  $K_xFe_{2-y}Se_2$  was prepared despite the presence of tetragonal FeSe. The implication of these results are that this hydrothermal route can lead to pure 122 type of layered compounds or the corresponding deintercalated tetragonal system. In addition, this hydrothermal route can be advantageous over solid-state route to avoid high temperature impurity phases or targeting compounds not thermodynamically stable at low temperature.

## More notes on the structure of Na-Tochinilite

A projection of Fe atoms on the (001) plane in Na-tochinilite is illustrated in Fig. S5, and compared to perfect square lattice in tetragonal FeS, there is a clear distortion along the  $b$ -axis.

The comparison between the morphologies of  $(Li_{1-x}Fe_xOH)FeS$  and NaOH intercalated FeS systems may provide further evidence of the hexagonal hydroxide layers with the NaOH reactions. Our  $(Li_{1-x}Fe_xOH)FeS$  samples consisted mainly of square-shaped platelets in micron size (Fig. S6a and Fig. S6b), which would be indicative of the underpinning layered tetragonal structure. However, a similar morphology was not observed for either the *inc*-Na-tochinilite or Na-tochinilite samples (Fig. S6c and Fig. S6d, respectively). While still layered, the crystallites display irregular shapes instead of square platelets. Their lack of either long-range tetragonal or hexagonal symmetry seems to be corroborate their morphologies.

Table S1: Rietveld refinement of synchrotron PXRD data collected at room temperature for a superconducting sample of  $(Li_{1-x}Fe_xOH)FeS$  shown in Fig. 3a and a non-superconducting sample shown in Fig. 3b. Both samples are fitted to a  $P4/nmm$  space group with 2 formula units in each unit cell ( $Z = 2$ ). The tetrahedral angles  $\alpha_1$  and  $\alpha_2$  represent the S-Fe-S angles in and out of the basal plane, respectively.

$a = 3.7041(1) \text{ \AA}, c = 8.8877(1) \text{ \AA} \text{ , } R_{wp} = 14.27\%, T_c = 3 \text{ K}$						
Atom	Wyckoff site	$x$	$y$	$z$	Occ.	$U_{iso} (\text{\AA}^2)$
Li/Fe1	2b	0	0	0.5	0.848/0.152(1)	0.0398(11)
Fe2	2a	0.5	0.5	0	1	0.0091(2)
O	2c	0.5	0	0.4184(3)	1	0.0174(7)
S	2c	0	0.5	0.1444(2)	1	0.0104(3)
$\alpha_1 (^\circ)$	$\alpha_2 (^\circ)$	Fe-Fe (Å)	Fe-S (Å)	F.U.		
110.55(5)	108.93(3)	2.6192(1)	2.2534(7)	(Li <sub>0.85</sub> Fe <sub>0.15</sub> OH)FeS		
$a = 3.7011(1) \text{ \AA}, c = 8.9257(1) \text{ \AA} \text{ , } R_{wp} = 10.91\%, \text{ non-superconducting}$						
Atom	Wyckoff site	$x$	$y$	$z$	Occ.	$U_{iso} (\text{\AA}^2)$
Li/Fe1	2b	0	0	0.5	0.846/0.154(1)	0.0380(7)
Fe2	2a	0.5	0.5	0	1	0.0092(1)
O	2c	0.5	0	0.4182(2)	1	0.0141(5)
S	2c	0	0.5	0.1439(1)	1	0.0102(2)
$\alpha_1 (^\circ)$	$\alpha_2 (^\circ)$	Fe-Fe (Å)	Fe-S (Å)	F.U.		
110.47(3)	108.98(2)	2.6171(1)	2.2527(4)	(Li <sub>0.85</sub> Fe <sub>0.15</sub> OH)FeS		

Table S2: List of  $\text{Li}_{1-x}\text{Fe}_x\text{OH})\text{FeS}$  samples. Detailed synthetic conditions are described in the above text, and only temperature, the most important factor, is shown in the table. Lattice constants of only representative samples are shown for duplicate samples. Because Na-tochilinite can be produced with the presence of NaOH,  $\text{Na}_2\text{S} \cdot 9\text{H}_2\text{O}$  was not used as a precursor for powder samples due to its hydrolysis to NaOH and NaSH in solution.  $\text{Li}_2\text{S}$  was the main sulfur source used for powder samples, and every sample prepared with  $\text{Li}_2\text{S}$  has been reproduced at least once. Single crystal samples are not very homogeneous, and their  $T_c$ 's vary from crystal to crystal, but their superconductivity is highly reproducible. Multiple single crystal batches have been reproduced at 120 °C using different sulfur sources with the presence of Sn.

	No.	Temperature (°C)	Sulfur source	Sn (Y/N)	$T_c$ (K)	$a$ (Å)	$c$ (Å)
Powder	1	130	$\text{Li}_2\text{S}$	N	N/A	3.706	8.862
	2	160	$\text{Li}_2\text{S}$	N	N/A	3.704	8.942
	3	160	thiourea	N	N/A	3.696	8.979
	4	180	thiourea	N	N/A	3.702	8.943
	5	200	thiourea	N	N/A	3.702	8.970
	6	120	thiourea	Y	2-3	3.700	8.919
	7	120	$\text{Li}_2\text{S}$	Y	2-3	3.704	8.900
	8	140	$\text{Li}_2\text{S}$	Y	2-3	3.706	8.900
	9	160	$\text{Li}_2\text{S}$	Y	2-3	3.704	8.888
	10	200	$\text{Li}_2\text{S}$	Y	N/A	3.701	8.926
SC	11	120	thiourea	Y	2-8	3.703	8.935
	12	120	$\text{Na}_2\text{S} \cdot 9\text{H}_2\text{O}$	Y	2-6	3.712	8.877
	13	120	$\text{Li}_2\text{S}$	Y	2-4	3.703	8.960



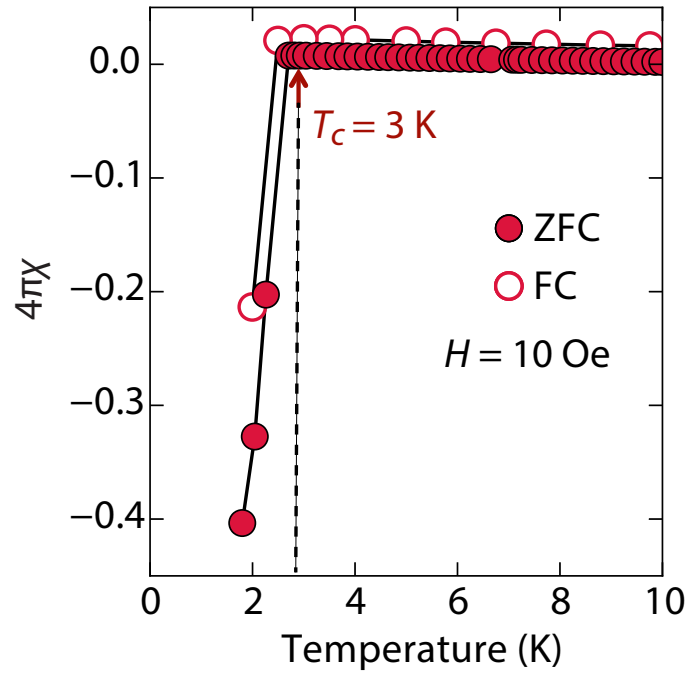


Figure S1: Temperature dependent magnetic susceptibility measurement of superconducting  $(\text{Li}_{1-x}\text{Fe}_x\text{OH})\text{FeS}$ . The XRD pattern of this sample is shown in Fig. 3a

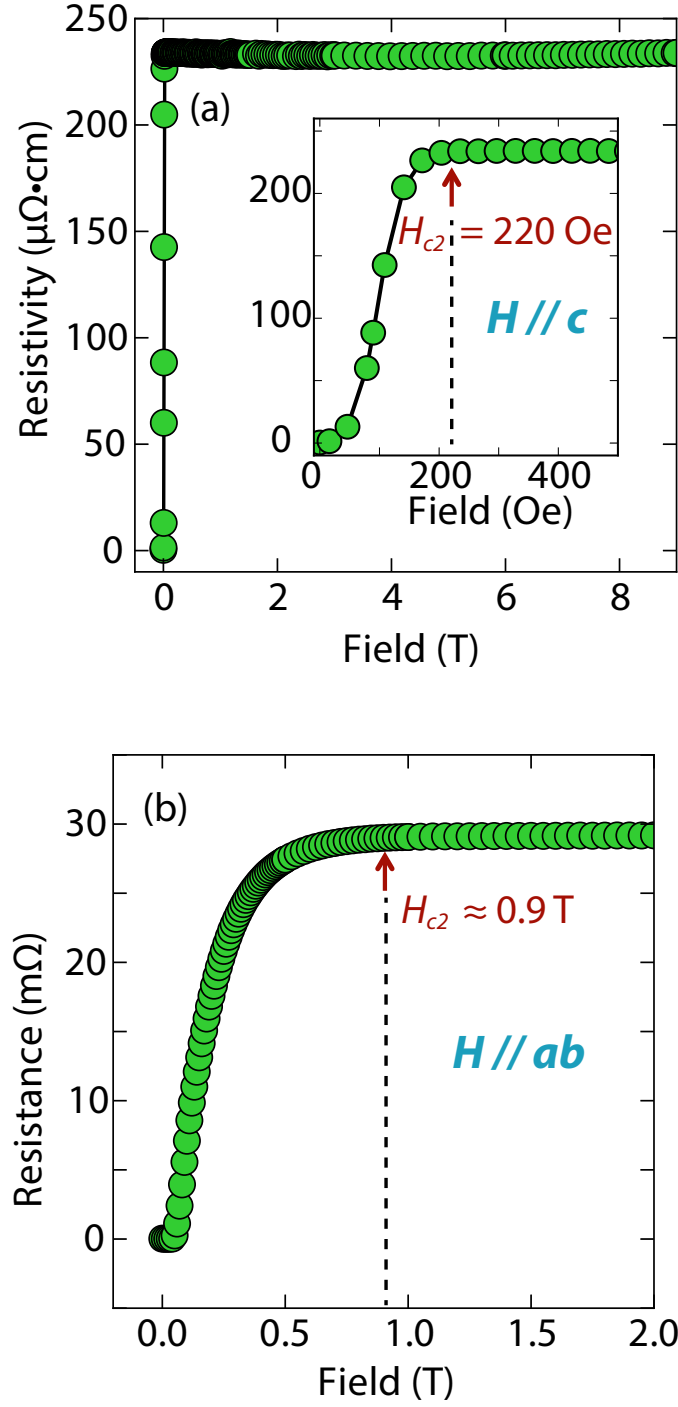


Figure S2: Field dependence of electrical resistance for a superconducting  $(\text{Li}_{1-x}\text{Fe}_x\text{OH})\text{FeS}$  sample ( $T_c = 3.5$  K) at 1.8 K. The anisotropy of  $H//c$  and  $H//ab$  are shown in (a) and (b), respectively. Its temperature dependent electrical resistivity is shown in Fig. 2a.

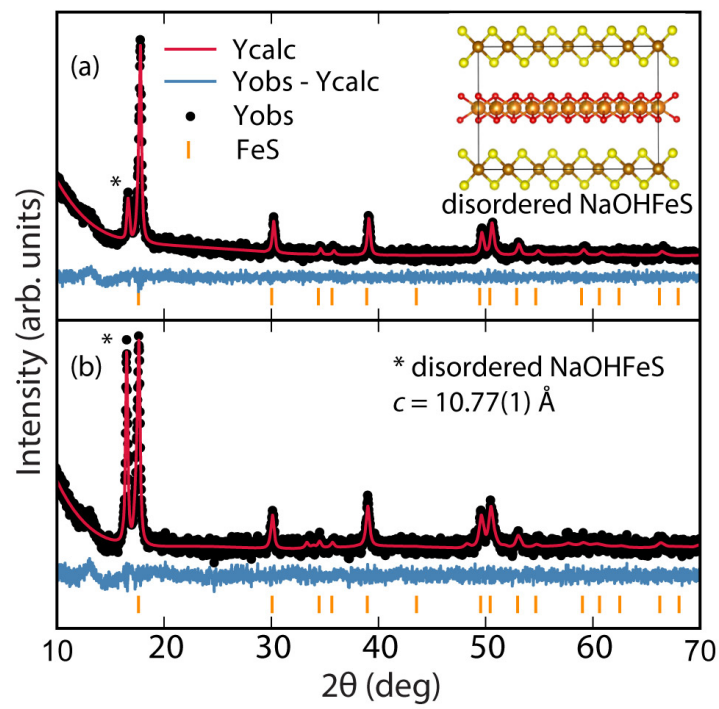


Figure S3: XRD patterns of mixtures of disordered NaOH intercalated FeS (indicated by \*) and tetragonal FeS (indicated by tick marks) with significantly more tetragonal FeS in (a) than (b). The magnetic susceptibility of (a) and (b) are shown in Fig. S4 and Fig. 4, respectively.

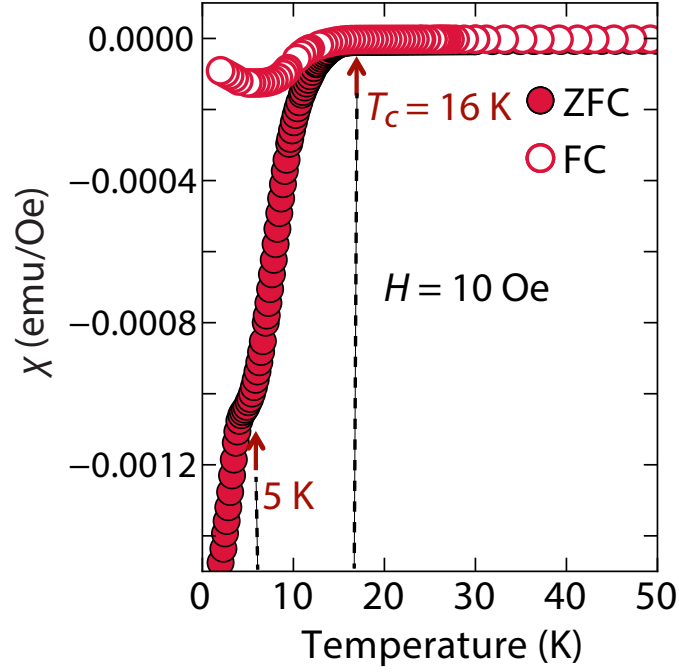


Figure S4: Temperature dependent magnetic susceptibility measurement of *inc*-Na-tochilinite with tetragonal FeS as a major phase. Its XRD pattern is shown in Fig. S3a

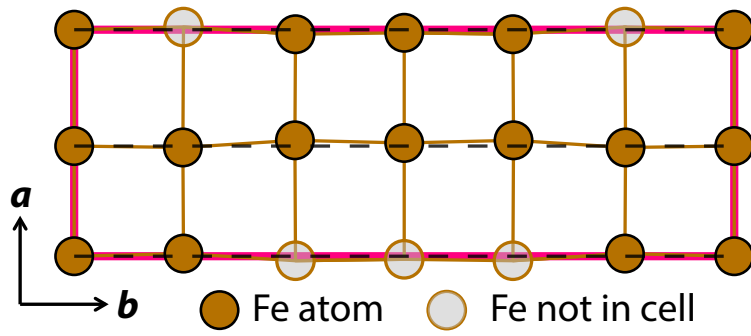


Figure S5: A projection of the Fe atoms on the (001) plane of the naturally occurring mineral tochilinite,  $(2(\text{Fe}_{1-x}\text{S}) \cdot 1.8[(\text{Mg}, \text{Fe})(\text{OH})_2])$ . A similar distortion of FeS square lattice is observed for Na-tochilinite as suggested by electron diffraction.

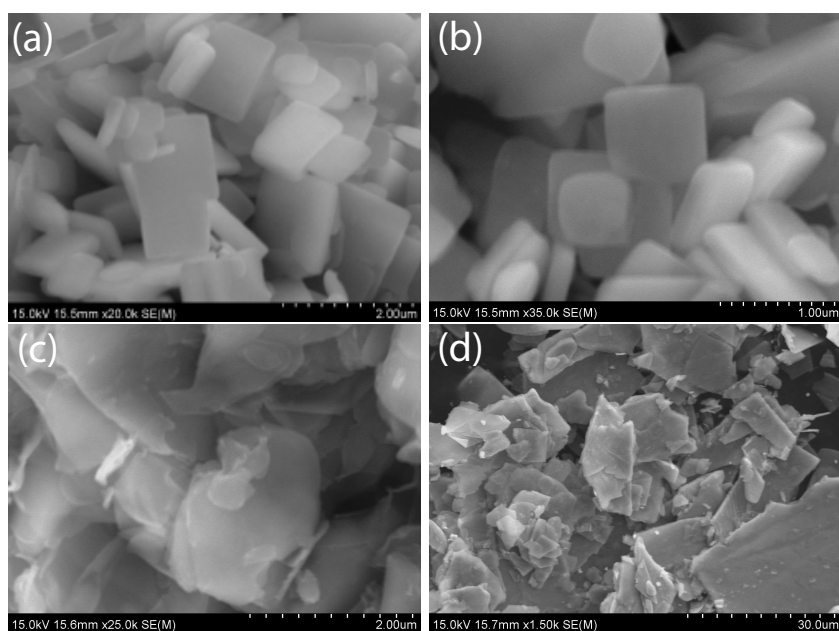


Figure S6: Scanning electron microscopy (SEM) images of (a) and (b)  $(\text{Li}_{1-x}\text{Fe}_x\text{OH})\text{FeS}$ , (c) *inc*-Na-tochilinite and (d) Na-tochilinite